Extremely Stable Platinum Nanoparticles Encapsulated in a Zirconia Nanocage by Area-Selective Atomic Layer Deposition for the Oxygen Reduction Reaction

Niancai Cheng, Mohammad Norouzi Banis, Jian Liu, Adam Riese, Xia Li, Ruying Li, Siyu Ye, Shanna Knights, and Xueliang Sun*

Polymer electrolyte fuel cells (PEFCs) are promising alternative power sources for transportation and portable applications due to their high efficiency, near room temperature operation, and zero emissions.[1] Pt is the most effective catalyst to facilitate both hydrogen oxidation and oxygen reduction in PEFCs.[2] In order to effectively utilize this expensive metal, Pt nanoparticles (NPs) are often supported on substrates such as oxides and carbon materials. However, Pt catalysts at the cathode operate under severe conditions, such as low pH (<1), high oxygen concentration, high humidity, and at high potentials (≈0.6–1.2 V).[3] Pt catalysts are thus seriously deactivated under such severe conditions, resulting in the loss of Pt performance due to Pt NP agglomeration caused by easy migration of the particles on the supports.[1c,4] The inherently sluggish kinetics of the oxygen reduction reaction (ORR) and instability of Pt at the cathode are the big challenges for widespread commercialization of PEFCs.[5] Thus, there is a significant need for highly active and durable Pt catalysts that can withstand the harsh conditions and prevent performance loss due to particle migration and agglomeration.

The migration of supported metal NPs can be inhibited through steric stabilization by layers of porous inorganic oxide such as zirconia,[6] silica,[7] or tin oxide.[8] This is an attractive way to enhance the stability of metal NPs. However, it is still challenging to precisely control the thickness of porous overlayers, and the poorly porous layers lead to a decrease in catalytic activity from mass transfer resistance.[9] In addition, the poor porous layers cover some surface of the catalyst, resulting in a loss of catalytic activity. Recently, porous alumina layers deposited by atomic layer deposition (ALD) have gained considerable attention,[10] because it can precisely control alumina layer thickness to stabilize supported metal particles based on sequential and self-limiting surface reactions.[9,11] However, alumina is unsuitable for many applications because it is an amphoteric substance, which reacts with both acids and bases. To achieve superior control using ALD, area-selective deposition can be done, taking advantage of the high sensitivity of the process to substrate surface conditions.[11b,12] Doing this requires surface functional groups to be manipulated or patterned in advance of material deposition, resulting in area-selective ALD. The materials are deposited only where needed using area-selective ALD, which avoids blocking the active site of catalysts by deposited materials.

The use of highly stable supports is another way to improve Pt stability. Numerous investigations have been carried out to improve the activity and durability of Pt catalysts. For instance, much effort has been devoted to develop novel durable catalyst support materials such as nitrogen-doped carbon nanotube (NCNT),[13] and ceramic support.[1c,14] Recently, NCNTs have been reported as support materials in fuel cell catalysts.[5b,15] NCNTs not only exhibit higher electrochemical corrosion resistance than carbon black[13] but also improve Pt catalytic activity toward ORR.[16] In addition, it has been proven that the NCNT can favor the ALD process due to their defective surface, which is an ideal support for the growth of ALD metal or metal oxide.[17]

Here, we demonstrate a facile approach to stabilize Pt catalysts encapsulated in stable zirconia nanocages by area-selective ALD. The Pt NPs were encapsulated in zirconia nanocages to enhance Pt stability and activity. An outline of the synthetic strategy for the Pt encapsulated in zirconia nanocage is depicted in **Figure 1**. Pt NPs were initially deposited on NCNT by ALD, followed by the application of a blocking agent (oleylamine) to the Pt NPs surface. ALD zirconia selectively grew around the Pt NPs, but was not deposited on the Pt surface due to the blocking agent. A nanocage structure may be formed by precisely controlling the ALD metal oxide layers. The prepared Pt catalyst encapsulated in zirconia nanocages showed very high stability and activity toward oxygen reduction.

A Pt/NCNT catalyst was prepared by 100 ALD cycles, resulting in highly disperse and uniform Pt NPs on the support surface. The Pt particles were about 1–3 nm in diameter with an average size of 1.8 nm (Supporting Information, Figure S1). The morphology of ALD ZrO_2 with different cycles on Pt/NCNT is shown in **Figure 2**. At 20 cycles of ALD ZrO_2, the ZrO_2 NPs grew around the Pt NPs and were not directly deposited on Pt surface due to the blocking agent (Figure 2a–c). With 30 cycles, the ZrO_2 NPs grew larger (Figure 2d–f), while the nanocage structure formed at 50 cycles (Figure 2g–i). An open, or holey nanocage can be formed through the precise

Dr. N. Cheng, Dr. M. N. Banis, Dr. J. Liu,
A. Riese, X. Li, R. Li, Prof. X. Sun
Department of Mechanical and Materials Engineering
University of Western Ontario
London, Ontario N6A 5B9, Canada
E-mail: xsun@eng.uwo.ca
Dr. S. Ye, S. Knights
Ballard Power Systems Inc.
9000 Glenlyon Parkway
Burnaby, British Columbia V5J 5J8, Canada

**ADVANCED
MATERIALS**

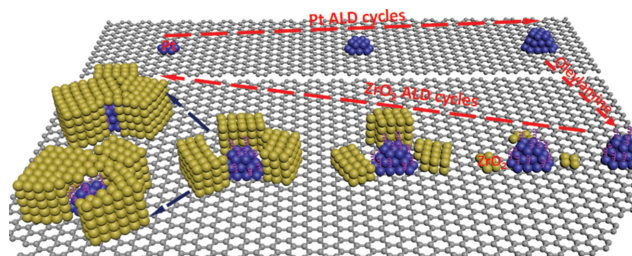www.advmat.de

*Materials
Views*

www.MaterialsViews.com

Figure 1. Schematic diagram of platinum encapsulated in zirconia nanocages structure fabricated by area-selective ALD.

control achieved by ALD cycling, as shown in Figure 1. The holey nanocages (marked with white circles) were found from HRTEM image, as shown in Figure 2h,i. The ZrO_2-Pt structures were further characterized using scanning transition electron microscopy (STEM) with energy dispersive X-ray spectroscopy (EDX) and EDS line-scanning. It was observed that white spots are Pt NPs surrounded by light grey ZrO_2 on the surface of NCNT (Supporting Information, Figure S2). The EDX line-scanning further confirmed that the light gray ZrO_2 is around the white Pt NPs (Supporting Information, Figure S3).

The thermal stability of ALD ZrO_2-Pt/NCNT catalysts with different ALD cycles of ZrO_2 was studied by subjecting the samples to calcination at temperatures of 400 and 600 °C for 2 h. From STEM images, it is obvious that the sinter resistance of the supported Pt NPs was enhanced with the coverage of ZrO_2 (Supporting Information, Figure S4). For ALD20ZrO_2-Pt/NCNT, the average size of Pt NPs increased from 1.8 nm to about 3.6 nm and 4.2 nm at 400 and 600 °C for 2 h, respectively (Figure S4b,c). The average size of Pt NPs increased slightly to 2.3 and 2.7 nm for ALD30ZrO_2-Pt/NCNT at 400 and 600 °C, respectively (Figure S4e,f). For ALD50ZrO_2-Pt/NCNT,

however, the supported Pt NPs were successfully stabilized up to 600 °C (Figure S4h,i), as demonstrated by retaining their average particle size of 2.0 nm. This clearly indicated that the zirconia nanocage can effectively prevent supported NPs from sintering and agglomeration. The XRD data (Supporting Information, Figure S5) showed that ALDPt NPs have a face-centered cubic (fcc) crystal structure[18] and zirconia nanocage is the tetragonal crystalline ZrO_2, which is consistent with the results of previous work.[17c]

We investigated the effects of the zirconia nanocage structure on ALDPt/NCNT electrochemical stability for use as catalysts for ORR in PEFCs. The prepared catalysts were tested in an acidic solution and compared with benchmarks of ALDPt/NCNT without zirconia nanocage and commercial Pt on carbon black catalyst (E-TEK 30%Pt/C). The accelerated durability tests (ADT) of the catalysts were conducted using a thin-film catalyst deposited onto a glassy carbon rotating-disk electrode. The electrode potential was cycled between 0.6 and 1.2 V versus RHE at a scan rate of 50 mV s^{-1} in O_2-staturated 0.5 M H_2SO_4 electrolyte. The electrochemical surface area (ECSA) of the Pt after potential cycling was calculated for each sample from their CVs (Supporting Information, Figure S6a–c) and plotted as a function of the cycle number (**Figure 3**a). Interestingly, the Pt activity of ALD50ZrO_2-Pt/NCNT600 °C catalysts increased with the potential cycling and revealed the highest activity after 500 potential cycling due to the surfaces of Pt NPs covered with impurities such as carbon resulting from removal of blocking agent on Pt surface. The impurities on the Pt metal surface were removed during potential cycling.[19] After 4000 cycles, the ALD50ZrO_2-Pt/NCNT600 °C catalysts lost only about 8% of its initial ECSA, whereas the ALDPt/NCNT without ALDZrO_2 deposition lost almost 74% of its initial Pt ECSA. The ECSA of the Pt/C catalyst decreased by 82% with the same cycling. This finding demonstrated that the ALD50ZrO_2-Pt/NCNT600 °C catalyst was nine times and ten times more stable than ALDPt/NCNT and Pt/C catalysts, respectively. ALD50ZrO_2-Pt/NCNT600 °C catalysts also show higher stability compared with other reported catalysts, as shown in Figure S7 in the Supporting Information. The high stability of Pt NPs encapsulated in zirconia nanocage should be attributed to the unique structure of the catalyst in this work. The detailed advantage of the structure of Pt NPs encapsulated in zirconia nanocage will be discussed subsequently.

The ORR activities were also measured for all catalysts in O_2-saturated 0.5 M H_2SO_4 electrolyte before and after ADT (Figure 3b,c, and Supporting Information, Figure 6Sd,e). The ORR mass activity (based on Pt loading) of the tested catalysts were calculated and are shown in Figure 3b. For fresh catalysts, the ORR specific activity of different catalysts increases in the order Pt/C < ALDPt/NCNT < ALD50ZrO_2-Pt/NCNT600 °C at 0.90 V versus RHE. The ALD50ZrO_2-Pt/NCNT600 °C catalyst exhibited a mass activity of 0.28 A m g^{-1} at 0.9 V, which was 1.4 and 6.4 times
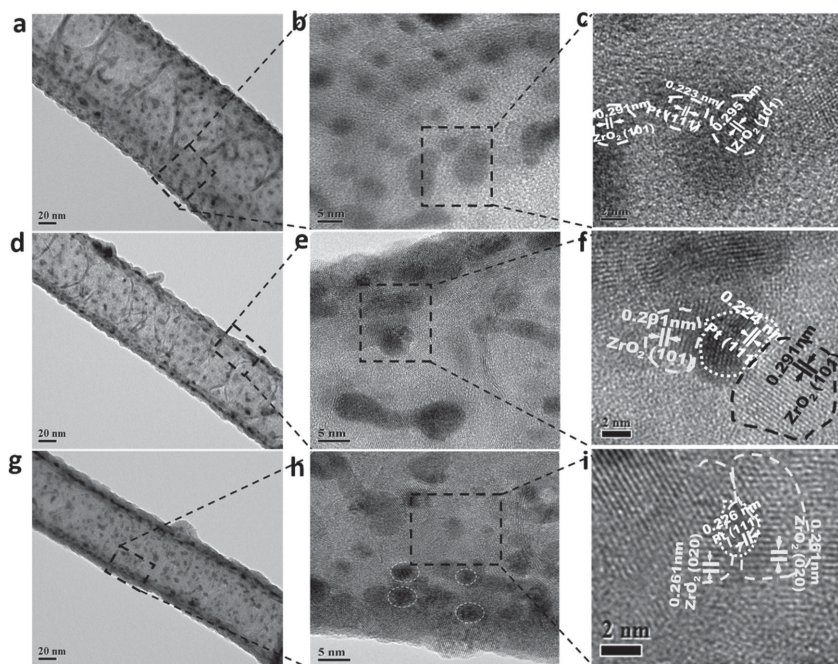

Figure 2. a,d,g) TEM and b,c,e,f,h,i) HRTEM images of ALD ZrO_2-Pt/NCNT catalysts with (a–c) 20 cycles, (d–f) 30 cycles, and (g–i) 50 cycles of ALD ZrO_2.
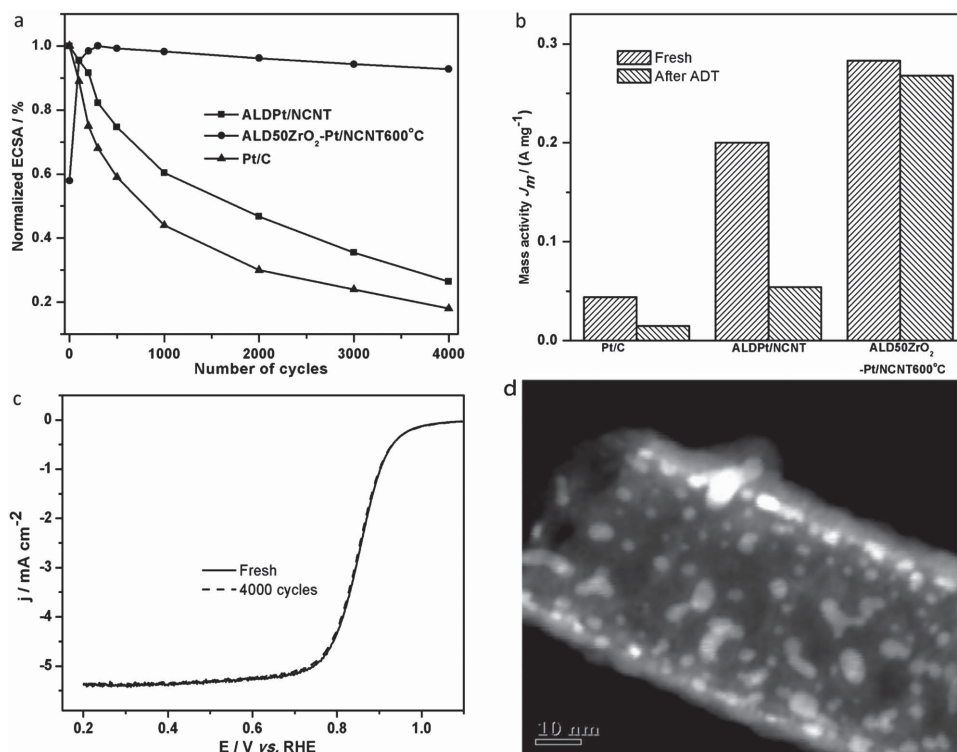
Materials
Views
www.MaterialsViews.com

ADVANCED
MATERIALS
www.advmat.de

COMMUNICATION

Figure 3. a) Loss of electrochemical surface area (ECSA) of ALDPt/NCNT, ALD50ZrO$_2$-Pt/NCNT600 °C, and E-TEK Pt/C catalysts as a function of cycling numbers. b) Mass activity at 0.9 V (vs RHE) for ALD Pt/NCNT, ALD50ZrO$_2$-Pt/NCNT600 °C, and E-TEK Pt/C catalysts. ALD Pt/NCNT and E-TEK Pt/C catalysts after 50-cycle electrochemical activation act as fresh catalysts. ALD50ZrO$_2$-Pt/NCNT600 °C after 500-cycle electrochemical activation acts as a fresh catalyst. c) ORR curves of electrodes made from ALD50ZrO$_2$-Pt/NCNT600 °C in an O$_2$-saturated 0.5 M H$_2$SO$_4$ solution at room temperature (1600 rpm, sweep rate: 10 mV s^{-1}) during the durability tests. d) STEM image of ALD50ZrO$_2$-Pt/NCNT600 °C after ADT.

greater than that of ALDPt/NCNT (0.20 A m g^{-1}) and Pt/C (0.044 A m g^{-1}), respectively. Figure S6 in the Supporting Information shows the polarization curves of the ALDPt/NCNT (Figure S6d) and Pt/C (Figure S6e) catalysts that clearly indicate a considerable current drop after the ADT, while there is almost no change for ALD50ZrO$_2$-Pt/NCNT600 °C (Figure 3c). After ADT, the mass activity of ALD50ZrO$_2$-Pt/NCNT600 °C at 0.9 V is 0.27 A m g^{-1}, while ALDPt/NCNT and Pt/C have 0.054 and 0.015 A m g^{-1} (Figure 3b). The mass activity of ALD50ZrO$_2$-Pt/NCNT600 °C is almost 5 and 18 times higher than that of Pt/NCNT and Pt/C catalysts, respectively, after ADT.

The morphology changes of the ALD50ZrO$_2$-Pt/NCNT600 °C, ALDPt/NCNT, and Pt/C catalysts after ADT were examined by TEM and STEM. After ADT, the size of the Pt NPs in the Pt/C catalyst increased from 3.9 to 8.1 nm (Supporting Information, Figure S8), indicating that serious ripening or aggregation of the Pt NPs occurred during the CV cycling. The average Pt particle size of ALDPt/CNT was changed from 1.8 to 6.5 nm during the durability tests (Supporting Information, Figure S9). In contrast, after ADT, the size of the Pt NPs in the ALD50ZrO$_2$-Pt/NCNT600 °C was 2.2 nm and underwent almost no change (Supporting Information, Figure S4i and Figure 3d), suggesting that the zirconia nanocages stabilized the Pt NPs during potential cycling.

Using area-selective ALD-synthesized ZrO$_2$ nanocage is a very effective approach to stabilize Pt NPs based on the results from the thermal stability and electrochemical stability tests.

However, it is very important to precisely control the thickness of ZrO$_2$ to form a holey nanocage by ALD. A nanocage structure, with holes, can be synthesized through 50 ALD cycles. The closed nanocage can be formed with increase in ALD cycles, which decrease the Pt activity (Supporting Information, Figure S10 and S11). As shown in Figure S10, the deposited ZrO$_2$ almost totally covered the surface of ALDPt/NCNT and closed nanocage formed at 90 cycles. The closed metal oxide nanocage hinders reactants such as oxygen and protons to reach the surface of the Pt catalyst, resulting in the low activity of Pt catalysts as shown in Figure S11. In addition, the annealing temperature affects the stability of Pt NPs encapsulated in zirconia nanocage, as shown in Figure S12 in the Supporting Information, because the annealing procedure can smooth out the surface of the catalyst to remove the defects or the under-coordinated sites most prone to corrosion.[20] The blocking agent also plays a very important role on activity of Pt. When direct deposition of ZrO$_2$ on ALDPt/NCNT without agent block, the deposited ZrO$_2$ block some of the active site of Pt NPs, leading to a decrease in the activity of Pt NPs although improved durability of Pt catalysts (Supporting Information, Figure S13).

Previous studies have been shown that metal oxides not only improve the activity of Pt NPs toward ORR due to synergetic effects between Pt and metal oxides[1c,21] but also enhance the durability of Pt catalysts through the strong metal support interactions with Pt.[22] Compared with ALDPt/NCNT and Pt/C catalysts, the enhanced activity of Pt encapsulated in

ZrO_2 nanocages can be attributed to the small size Pt NPs and the synergetic effects of Pt and ZrO_2. In general, the Pt ECSA decreases through: i) Ostwald ripening, i.e., dissolution of the cationic Pt species from the small Pt metal particles and redeposition on large metal particles,[3b] ii) coalescence of Pt NPs by Pt nanocrystal migration because of weak interactions between Pt and support,[23] and iii) Pt NP agglomeration caused by corrosion of the support material.[22b,22c] Compared with ALDPt/NCNT and Pt/C catalysts, the increased stability of ALD50ZrO2-Pt/NCNT600 °C should be attributed to the presence of the zirconia nanocage. The Pt NPs were encapsulated in nanocages, which could prevent the Pt NPs migration and agglomeration due to the otherwise weak interaction of Pt NPs and support, and corrosion of the support material. In addition, the diffusion of dissolved Pt species out of the zirconia nanocage can be prevented and instead the dissolved Pt species redeposit on the original Pt metal particles due to the Pt metal particles encapsulated in the zirconia nanocage during potential cycling.[7c] Furthermore, as discussed above, the annealing procedure can smooth out the surface of the catalyst to remove the defects or the undercoordinated sites most prone to corrosion.[20]

In summary, we have demonstrated a facile approach to stabilize Pt catalysts encapsulated in a zirconia nanocage by area-selective ALD. The Pt NPs encapsulated in the zirconia nanocage indicated very high stability and activity toward the ORR in acidic media. Pt NPs encapsulated in a zirconia nanocage show nine and ten times more stability than ALDPt/NCNT and Pt/C catalysts, respectively. Our novel catalyst also exhibited an ORR activity 1.4 and 6.4 times greater than that of ALDPt/NCNT and Pt/C, respectively. These remarkable improvements in stability in this novel catalyst are attributed to the presence of the zirconia nanocages, which prevent Pt NP migration and agglomeration on the support. In addition, it is suggested that the enhanced activity of Pt encapsulated in zirconia nanocages was mainly due to the small size Pt NPs and the synergetic effects of Pt and ZrO_2. Additionally, the catalyst of Pt NPs encapsulated in the zirconia nanocage exhibited significantly enhanced resistance to sintering up to 600 °C. We believe that the general synthetic strategy presented here can be extended to other catalytic systems with different compositions.

Supporting Information

Supporting Information is available from the Wiley Online Library or from the author. Experimental details and additional results are included.

Acknowledgements

[1] a) D. L. Wang, C. V. Subban, H. S. Wang, E. Rus, F. J. DiSalvo, H. D. Abruna, *J. Am. Chem. Soc.* **2010**, *132*, 10218; b) T. Fujigaya, N. Nakashima, *Adv. Mater.* **2013**, *25*, 1666; c) Y. J. Wang, D. P. Wilkinson, J. J. Zhang, *Chem. Rev.* **2011**, *111*, 7625; d) Y. Y. Shao, G. P. Yin, Y. Z. Gao, *J. Power Sources* **2007**, *171*, 558.

[2] J. N. Tiwari, K. Nath, S. Kumar, R. N. Tiwari, K. C. Kemp, N. H. Le, D. H. Youn, J. S. Lee, K. S. Kim, *Nat. Commun.* **2013**, *4*, 2221.

[3] a) L. M. Roen, C. H. Paik, T. D. Jarvic, *Electrochem. Solid-State Lett.* **2004**, *7*, A19; b) P. J. Ferreira, G. J. la O', Y. Shao-Horn, D. Morgan, R. Makharia, S. Kocha, H. A. Gasteiger, *J. Electrochem. Soc.* **2005**, *152*, A2256.

[4] Y. Shao-Horn, W. C. Sheng, S. Chen, P. J. Ferreira, E. F. Holby, D. Morgan, *Top Catal.* **2007**, *46*, 285.

[5] a) M. K. Debe, *Nature* **2012**, *486*, 43; b) S. Jiang, Y. Ma, G. Jian, H. Tao, X. Wang, Y. Fan, Y. Lu, Z. Hu, Y. Chen, *Adv. Mater.* **2009**, *21*, 4953; c) Y. Zheng, Y. Jiao, J. Chen, J. Liu, J. Liang, A. Du, W. M. Zhang, Z. H. Zhu, S. C. Smith, M. Jaroniec, G. Q. Lu, S. Z. Qiao, *J. Am. Chem. Soc.* **2011**, *133*, 20116; d) J. J. Duan, S. Chen, S. Dai, S. Z. Qiao, *Adv. Funct. Mater.* **2014**, *24*, 2072; e) Y. Bing, H. Liu, L. Zhang, D. Ghosh, J. Zhang, *Chem. Soc. Rev.* **2010**, *39*, 2184; f) R. Imbeault, A. Pereira, S. Garbarino, D. Guay, *J. Electrochem. Soc.* **2010**, *157*, B1051.

[6] P. M. Arnal, M. Comotti, F. Schuth, *Angew. Chem Int. Ed.* **2006**, *45*, 8224.

[7] a) P. Lu, C. T. Campbell, Y. Xia, *Nano. Lett.* **2013**, *13*, 4957; b) S. H. Joo, J. Y. Park, C. K. Tsung, Y. Yamada, P. D. Yang, G. A. Somorjai, *Nat. Mater.* **2009**, *8*, 126; c) S. Takenaka, H. Matsumori, K. Nakagawa, H. Matsune, E. Tanabe, M. Kishida, *J. Phys. Chem. C* **2007**, *111*, 15133.

[8] S. H. Lee, D. M. Hoffman, A. J. Jacobson, T. R. Lee, *Chem. Mater.* **2013**, *25*, 4697.

[9] J. Lu, B. Fu, M. C. Kung, G. Xiao, J. W. Elam, H. H. Kung, P. C. Stair, *Science* **2012**, *335*, 1205.

[10] a) C. Marichy, M. Bechelany, N. Pinna, *Adv. Mater.* **2012**, *24*, 1017; b) M. Knez, K. Niesch, L. Niinisto, *Adv. Mater.* **2007**, *19*, 3425.

[11] a) J. Lu, B. Liu, J. P. Greeley, Z. Feng, J. A. Libera, Y. Lei, M. J. Bedzyk, P. C. Stair, J. W. Elam, *Chem. Mater.* **2012**, *24*, 2047; b) J. L. Lu, J. W. Elam, P. C. Stair, *Acc. Chem. Res.* **2013**, *46*, 1806; c) J. Lu, K. B. Low, Y. Lei, J. A. Libera, A. Nicholls, P. C. Stair, J. W. Elam, *Nat. Commun.* **2014**, *5*, 3264.

[12] a) R. Chen, S. F. Bent, *Adv. Mater.* **2006**, *18*, 1086; b) M. J. Weber, A. J. M. Mackus, M. A. Verheijen, C. van der Marel, W. M. M. Kessels, *Chem. Mater.* **2012**, *24*, 2973; c) M. H. Park, Y. J. Jang, H. M. Sung-Suh, M. M. Sung, *Langmuir* **2004**, *20*, 2257; d) N. A. Ray, R. P. Van Duyne, P. C. Stair, *J. Phys. Chem. C* **2012**, *116*, 7748; e) K. Kim, H.-B.-R. Lee, R. W. Johnson, J. T. Tanskanen, N. Liu, M.-G. Kim, C. Pang, C. Ahn, S. F. Bent, Z. Bao, *Nat. Commun.* **2014**, *5*, 4781.

[13] Y. G. Chen, J. J. Wang, H. Liu, R. Y. Li, X. L. Sun, S. Y. Ye, S. Knights, *Electrochem. Commun.* **2009**, *11*, 2071.

[14] a) H. Lv, S. Mu, *Nanoscale* **2014**, *6*, 5063; b) P. Wu, H. F. Lv, T. Peng, D. P. He, S. C. Mu, *Sci. Rep.* **2014**, *4*, 3968; c) E. Antolini, E. R. Gonzalez, *Solid State Ionics* **2009**, *180*, 746.

[15] Z. Yang, H. G. Nie, X. Chen, X. H. Chen, S. M. Huang, *J. Power Sources* **2013**, *236*, 238.

[16] Y. G. Chen, J. J. Wang, H. Liu, M. N. Banis, R. Y. Li, X. L. Sun, T. K. Sham, S. Y. Ye, S. Knights, *J. Phys. Chem. C* **2011**, *115*, 3769.

[17] a) X. B. Meng, Y. Zhong, Y. F. Sun, M. N. Banis, R. Y. Li, X. L. Sun, *Carbon* **2011**, *49*, 1133; b) X. B. Meng, M. Ionescu, M. N. Banis, Y. Zhong, H. Liu, Y. Zhang, S. H. Sun, R. Y. Li, X. L. Sun, *J. Nanopart. Res.* **2011**, *13*, 1207; c) J. Liu, X. Meng, M. N. Banis, M. Cai, R. Li, X. Sun, *J. Phys. Chem. C* **2012**, *116*, 14656; d) J. Liu, Y. J. Tang, B. W. Xiao, T. K. Sham, R. Y. Li, X. L. Sun, *RSC Adv.* **2013**, *3*, 4492.

[18] N. C. Cheng, S. C. Mu, X. J. Chen, H. F. Lv, M. Pan, P. P. Edwards, *Electrochim. Acta* **2011**, *56*, 2154.

[19] S. Takenaka, H. Matsumori, H. Matsune, M. Kishida, *Appl. Catal., A* **2011**, *409*, 248.

[20] I. E. L. Stephens, A. S. Bondarenko, U. Gronbjerg, J. Rossmeisl, I. Chorkendorff, *Energy Environ. Sci.* **2012**, *5*, 6744.

[21] a) Y. Liu, W. E. Mustain, *J. Am. Chem. Soc.* **2013**, *135*, 530; b) X. Han, F. Cheng, T. Zhang, J. Yang, Y. Hu, J. Chen, *Adv. Mater.* **2014**, *26*, 2047.

[22] a) A. Kumar, V. Ramani, *ACS Catal.* **2014**, *4*, 1516; b) L. Zhang, L. Y. Wang, C. M. B. Holt, B. Zahiri, Z. Li, K. Malek, T. Navessin, M. H. Eikerling, D. Mitlin, *Energy Environ. Sci.* **2012**, *5*, 6156; c) S. Y. Huang, P. Ganesan, S. Park, B. N. Popov, *J. Am. Chem. Soc.* **2009**, *131*, 13898; d) K. Sasaki, L. Zhang, R. R. Adzic, *Phys. Chem. Chem. Phys.* **2008**, *10*, 159; e) M. N. Banis, S. Sun, X. Meng, Y. Zhang, Z. Wang, R. Li, M. Cai, T.-K. Sham, X. Sun, *J. Phys. Chem. C* **2013**, *117*, 15457; f) R. Kou, Y. Shao, D. Mei, Z. Nie, D. Wang, C. Wang, V. V. Viswanathan, S. Park, I. A. Aksay, Y. Lin, Y. Wang, J. Liu, *J. Am. Chem. Soc.* **2011**, *133*, 2541.

[23] a) Z. Z. Jiang, Z. B. Wang, Y. Y. Chu, D. M. Gu, G. P. Yin, *Energy Environ. Sci.* **2011**, *4*, 728; b) B. Y. Xia, B. Wang, H. B. Wu, Z. Liu, X. Wang, X. W. Lou, *J. Mater. Chem.* **2012**, *22*, 16499.